J Polym Res (2011) 18:2151–2159
DOI 10.1007/s10965-011-9625-3

ORIGINAL PAPER

Characterization of Nanocomposites of Poly(butylene adipate-co-terephthalate) blending with Organoclay

Jung-Hung Chen · Chin-Chi Chen · Ming-Chien Yang

Received: 31 December 2010 / Accepted: 2 May 2011 / Published online: 11 May 2011

Abstract Nanocomposites of poly(butylene adipate-co-terephthalate) (PBAT) with montmorillonite (MMT) nanoparticles were prepared via solution blending. Natural MMT was modified by octadecylamine (ODA). Intercalation of the organoclay in the PBAT matrix was studied by X-ray diffraction (XRD). The results from scanning electron microscope (SEM) showed that the surface morphology of nanocomposite of PBAT/ODA-modified MMT was smoother than that of PBAT/neat MMT. From the results of transmission electron microscope (TEM), the dispersion of ODA-modified MMT in the PBAT matrix was finer than that of neat MMT. The addition of organoclay can increase the cooling crystallization temperature of PBAT, as observed by differential scanning calorimetry (DSC). Furthermore, the addition of ODA-modified MMT can improve the thermal stability of PBAT nanocomposites, according to the results of thermogravimetric analyzer (TGA). The tensile strength was little affected, while the Young's modulus was increased with the clay content. The photo degradation and the hydrolysis of PBAT were reduced by the addition of MMT and ODA-modified MMT. Although the hydrophilicity was increased, the transmission of water vapor was reduced greatly by the addition of ODA-modified MMT.

J.-H. Chen
Graduate Institute of Engineering,
National Taiwan University of Science and Technology,
Taipei, Taiwan

C.-C. Chen · M.-C. Yang (✉)
Department of Materials Science and Engineering,
National Taiwan University of Science and Technology,
Taipei, Taiwan
e-mail: myang@mail.ntust.edu.tw

Keywords Poly(butylene adipate-co-terephthalate) · Montmorillonite · Nanocomposite · Thermal properties · Mechanical properties · Degradation

Introduction

Polymers have been used in a wide range of engineering applications due to their plasticity and viscoelasticity. However, the mechanical strength and thermal stability of polymers are usually lower than those of ceramics and metals. In practical applications, polymers are added with rigid inorganic fillers, such as clay, glass fiber, carbon black, metal or metal oxide, to form organic–inorganic hybrids to improve the physical properties of polymers [1–3] or to enhance electric conductivity [4–9] and decrease gas permeability [10]. The reinforcing effects of nanocomposites usually are depended on the nanostructure configuration and interfacial bonding between the filler and the polymer [11].

Nanocomposites exhibit special characteristics in mechanical, thermal, optical and physical and chemical properties [12], allowing these materials used extensively in automotive, packaging, and building industries [13]. In the research of nanocomposites, biodegradable polymer matrices have been attracting attention in recent researches concerning the domestic wastes [14–16]. The presence of nanofiller can affect the morphology and mechanical properties as well as the biodegradation rate of the biodegradable polymer [17].

Montmorillonite (MMT), a lamellar silicate, has attracted a significant amount of attention due to its environmentally friendliness, naturally abundance, and the improvement of various properties in comparison with neat biodegradable polymers [18]. Usually, the dispersion of MMT particles in a polymer matrix results in the formation of two types, intercalated and exfoliated nanocomposites. The addition of

small amount of MMT could affect the nucleation and the crystal growth of PBAT in the composites. Montmorillonites are naturally hydrophilic. Cationic modifiers can exchange the cations in the clay to increase the organophilic characteristics [14], namely, higher compatibility with organic polymers.

Poly(butylene adipate-*co*-terephthalate) (PBAT) provided by BASF and Eastman Chemical is a biodegradable polymer possessing excellent properties of softness and ductility suitable for food packaging and agricultural films [19]. The biodegradation behavior and properties of PBAT have been studied by several researches [20–23]. However, the application of this biodegradable polymer would be limited by the relatively high cost and poor mechanical properties. A way to reduce the overall material cost and enhance the mechanical properties is the combination of biodegradable polymers with cheap inorganic or organic fillers. Several studies have been conducted on the nanocomposite of PBAT/MMT. In particular, Someya et al. studied the mechanical properties and biodegradation of PBAT/MMT nanocomposites [18, 19]. Chivrac et al. studied the nanocomposites of PBAT by solvent and melt intercalated methods. They suggested that the incorporation of montmorillonite as a nanofiller can improve PBAT properties and thus increase the attractiveness of this biodegradable polymer [24]. Recently, Yang and Qiu reported the crystallization, thermal stability, and dynamic mechanical properties of the nanocomposite of PBAT and Cloisite 30B (an organo-modified MMT) [17].

This study is to investigate the nanocomposites based on PBAT and organo-modified MMT. The aims of this study are to evaluate the effect of organoclays on the morphology, mechanical properties, thermal degradation, and in addition, the water vapor transmission and the photo degradation. The latter two properties are important for packaging applications. In the literatures, the molecular chain scission occurred on the polymer surface under UV exposure that resulted in free radicals. The barrier characteristics of nanoclay could delay the penetration of free radicals into the matrix, which is typical to photo-degradation [25, 26]. In addition, better dispersion of clays in the polymer matrix would result in better barrier properties to prevents the transmission of moisture vapor through the polymer nanocomposite [27]. The results of this study would be useful for investigating the potential of such nanocomposite as packaging material.

Experimental

Materials

PBAT (Ecoflex ®) was purchased from BASF. Sodium montmorillonite with a cationic exchange capacity of 85 mEq/100 g was provided by Pai-Kong Nano Technology Co. Ltd. (Taoyuan, Taiwan). The surfactant used in this study, octadecylamine (ODA), was purchased from Acros, USA. The surfactant was reagent-grade and was used without further purification.

Preparation of organoclay

A quantity of 10 g of MMT was dispersed in 500 mL of deionized water and stirred with 500 rpm for 1 h. In this study, the molar ratio of exchangeable surfactant was calculated from cationic exchange capacity of montmorillonite. Typically, 8.5 mmol of ODA and 10 mL of 1 N HCl were added to 300 mL of deionized water to help the clay ionizing. This solution was then mixed with the MMT dispersion and stirred at 60 °C with 500 rpm for 6 h. Afterward the solution was filtered and the organoclay was washed thoroughly with deionized water three times to remove the residual metal ions and chloride ions. The filtrate was detected with 0.1 N $AgNO_3$ solution until no AgCl precipitation, ensuring complete removal of chloride ions. The organoclay after filtration was dried at 60 °C for 24 h. The dried organoclay was ground and screened with a 250-mesh sieve to obtain fine clay particles. The ODA-modified MMT was denoted as O-M.

Preparation of PBAT film

Firstly, 10 g of PBAT pellets were dissolved in 40 mL of chloroform under agitation at room temperature until completely dissolved to form a homogeneous polymer solution. A given amount of clay and organoclay were dispersed in 10 mL of chloroform for 24 h. The clay dispersion was added slowly to the PBAT chloroform solution while stirring continuously for 24 h, and then was poured onto a glass plate (15 cm in diameter) at room temperature. After exposing to air for 12 h, the resulting film was dried in an oven at 60 °C and then the residual chloroform was extracted with ethanol. Finally, the resulting film was dried at 60 °C in a vacuum oven for 24 h in order to remove the residual solvent. The composition of each sample was summarized in Table 1.

X-ray diffraction (XRD) analysis

The *d*-space of clay layers in the nanocomposites was measured using an X-ray diffractometer (M21X, MAC Science) of CuKα radiation with a wavelength of 0.154 nm at 35 kV and 40 mA. The X-ray diffractograms were monitored in diffraction angle 2θ from 3° to 10° with a scanning rate of 2°/min in the ambient temperature.

Transmission electron microscope (TEM) analysis

Transmission electron microscopy was performed using a field emission TEM (FETEM) (Tecnai F20 G2, Philips) with

Table 1 Compositions of the samples

Sample	Clay type	Clay content
PBAT	None	0%
PBAT/MMT1	Natural MMT	1 wt.%
PBAT/MMT5	Natural MMT	5 wt.%
PBAT/MMT10	Natural MMT	10 wt.%
PBAT/O-M1	ODA-modified MMT	1 wt.%
PBAT/O-M5	ODA-modified MMT	5 wt.%
PBAT/O-M10	ODA-modified MMT	10 wt.%

an accelerating voltage of 70 kV. The samples were sectioned into films of roughly 100 nm in thickness using an ultramicrotomy and then mounted on 200-mesh copper grids.

Thermal analysis

The thermal properties and crystallinity of nanocomposites were determined by differential scanning calorimetry (DSC) (Q1000, TA Instrument, USA). The temperature and energy readings were calibrated with indium before each measurement. Sample was heated first to 200 °C at a heating rate of 10 °C/min, and held for 5 min in the hermetic cell to remove the thermal history. The sample was then cooled at 10 °C/min to 50 °C, and reheated to 200 °C at 10 °C/min. All samples were scanned in nitrogen environment. The melting temperature and recrystallizing temperature of PBAT nanocomposites were determined based on the second heating cycles.

Thermogravimetric analysis

The thermal stabilities of PBAT and PBAT nanocomposites were analyzed using a thermogravimetric analyzer (910, DuPont) at a heating rate of 10 °C/min in a nitrogen atmosphere.

Tensile Test

Tensile test of PBAT nanocomposites were performed with a tensile tester, MTS 810, according to the standard method for testing the tensile properties of plastics (ASTM D638). The gap length was 50 mm, and the testing speed was 5 mm/min. The results reported were the average of three specimens.

Surface analysis

Field emission scanning electron microscope (FE-SEM) was used to observe the surface morphology. All samples were coated with gold and then observed under a JEOL JSM-5410 scanning electron microscope.

Ultraviolet degradation

A piece of the sample ($10\times10\times0.3$ mm^3) was exposed under an ultraviolet (UV) lamp (6 W) at the wavelength of 360 nm for 18 h. The distance between the UV lamp and samples was 7 cm. After exposure, the samples were washed with distilled water and dried in an oven at 60 °C for 24 h. The weight losses of the dried samples were determined, and the tensile test was performed as described in previous section to measure the stress retention (σ_R) after UV exposure. The stress retention (σ_R) was calculated as follows:

$$\sigma_R(\%) = (\sigma_t/\sigma_o) \times 100$$

where σ_o is the stress of the original sample, and σ_t is the stress of the samples after UV exposure.

Hydrolytic degradation

Pieces of films ($10\times10\times0.3$ mm^3) were immersed in 50 ml of 0.1 M NaOH solution. At a specified period, the sample was removed from solution and washed with distilled water for 30 min, and weighed after vacuum drying at 60 °C for 24 h.

Contact angle

The contact angle between water and the nanocopmposites surface was measured by a FAST/60 contact angle meter from GBX, France.

Water vapor transmission rate

The water vapor transmission of the nanocomposite film (0.3 mm in thickness) was measured by sealing a specimen to the open mouth of a cup containing water and placing the assembly into a controlled atmosphere (50% RH, 23 °C) according to ASTM E96 BW standard. The cup was turned upside-down to let the water in contact with the specimen. The water vapor transmission rate (WVTR) through the specimen to the controlled atmosphere was thus determined.

Results and discussion

Surface analysis

Figure 1(a) shows the surface morphology of nanocomposites. The interaction between clay and polymer matrix was improved by the modification of organic surfactants. The surface of nanocomposite with lower content of O-M was smoother with less porosity. The uniformity of the surface

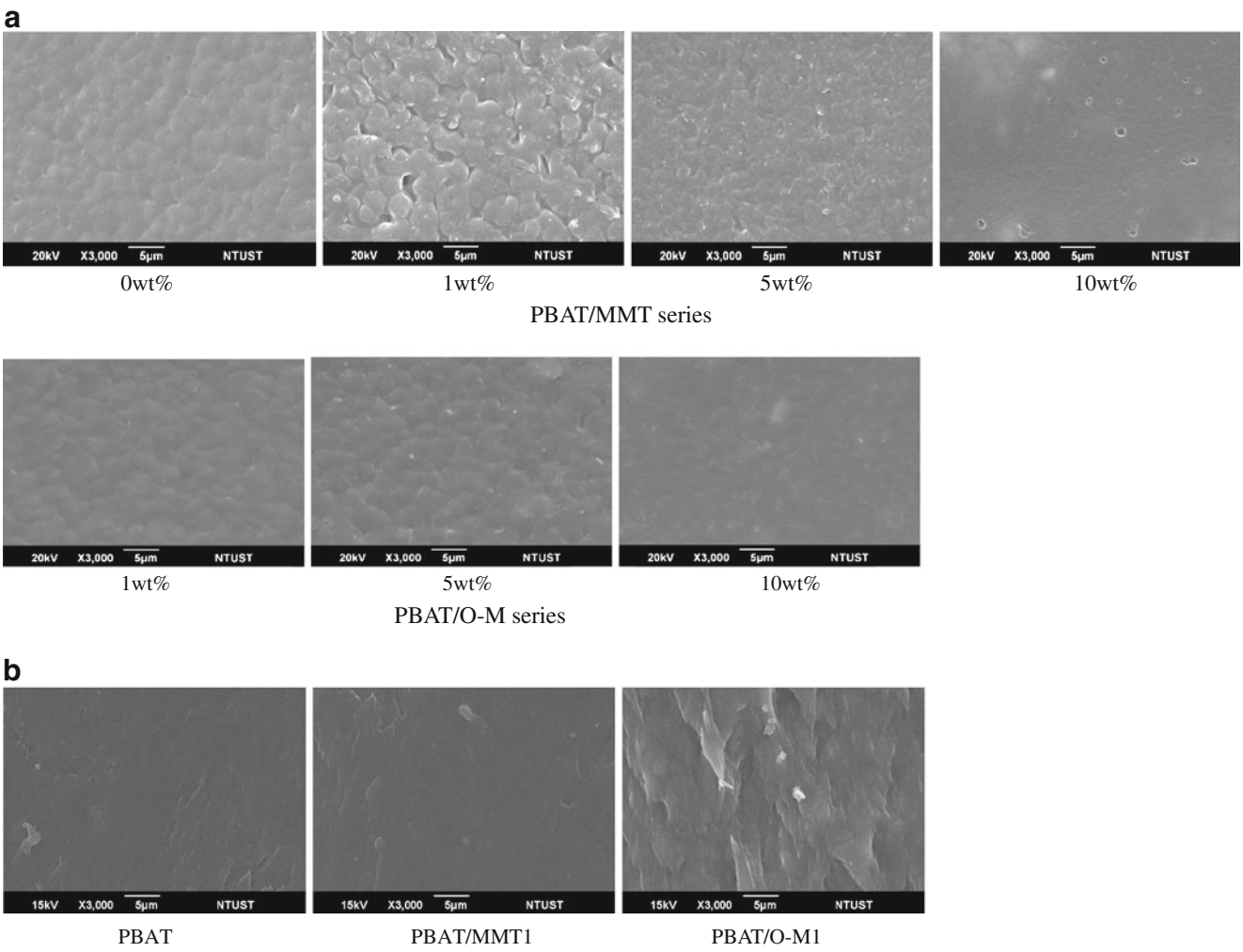

Fig. 1 **a** SEM micrographs of the surface morphology of PBAT nanocomposites with different clay/organoclay content. **b** SEM micrographs of the fracture surface morphology of PBAT and PBAT nanocomposites with 1 wt.% clay/organoclay content

was attributed to the homogeneous dispersion of organoclay in PBAT matrix. As the clay content increased, large pores were observed on the surface due to the uneven distribution of clay flakes caused by the aggregation resulted in different shrinkage stress between organoclay and polymer during solidification. The aggregation of clay flakes also resulted in the decrease of the tensile strength and elongation.

Figure 1(b) shows the fracture surface of neat PBAT and PBAT nanocomposites with 1 wt.% clay/organoclay. All the fracture surfaces were relatively smooth without pull-out, suggesting these samples were brittle. Because the particles were submicron in size, they were not observable at this magnification.

X-ray diffraction (XRD) analysis

Figure 2 shows the spectra of X-ray diffraction of MMT and PBAT nanocomposites containing MMT and O-M. The

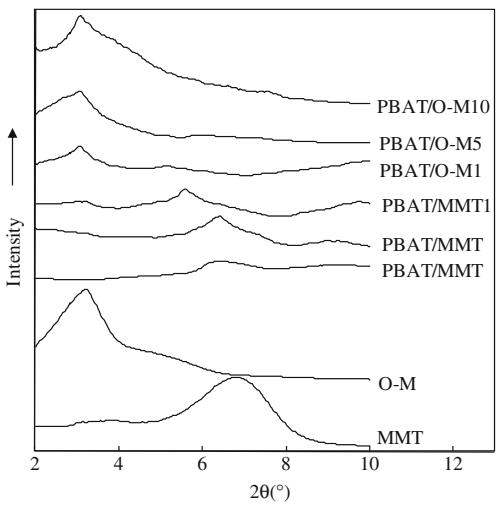

Fig. 2 Spectra of X-ray diffraction of MMT, O-M, PBAT and PBAT nanocomposites

peaks were corresponding to the crystalline structure of montmorillonite. The *d*-space between clay layers in PBAT matrix was calculated according to Bragg's law

$$\lambda = 2d\sin\theta$$

where λ is the wavelength of the X-ray radiation used (0.154 nm), *d* is the spacing between specific diffraction lattice planes and θ is the measured diffraction angle.

The results of *d*-space were summarized in Table 2. The organoclay expressed a smaller and sharper peak of 2θ than that of nature clay. For organoclay, the 2θ value of the peak shifted from 6.77 to 3.19 after ODA modified, indicating that the *d*-space was expanded to 2.77 nm as the sodium ions in the interlayer modified by ODA. Similar phenomenon was reported in the study by Jiang et al. [28]. However, the PBAT nanocomposites exhibited smaller 2θ values than pure clay and organoclay. This could be attributed to the partial intercalation of PBAT chains into the silicate galleries and resulted in the lager *d*-space. The peak of 2θ for PBAT nanocomposite containing 1 wt.% MMT was observed around 6.42°, which was corresponding to a *d*-space of about 1.38 nm. The smaller peak of 2θ of nanocomposites with organoclay was observed. For nanocomposite with 1 wt.% O-M organoclay, the smaller peak at 3.08° was corresponding to an interlayer spacing of 2.87 nm. This indicates that modification of clay with organic ions not only makes the clay surface hydrophobic but results in an increase of the *d*-space. The increase of *d*-space between clay and organoclay nanocomposites was attributed to the intercalation of ammonium surfactant. The surfactant having bulkier substitutent on the nitrogen atom resulted in a larger *d*-space [18]. However, a broader peak around 3.04° in the spectrum of nanocomposite with 1 wt.% O-M was observed. The phenomenon was attributed to that a huge amount of clay layers intercalated in PBAT matrix. The clay layers in PBAT matrix is presumed to form larger *d*-space and result in smaller scattering. The clear and shaper peak of 2θ of PBAT nanocomposites was observed with increasing organoclay content. This may be due to the formation of partially intercalated nanocomposite. This point is supported by the TEM images of PBAT nanocomposites with inorganic content 5 wt.% shown in Fig. 3. The PBAT nanocomposites with MMT exhibited some clusters of clays in contrast to that with O-M exhibiting more finely dispersed in the PBAT matrix. Figure 3 also shows that the PBAT nanocomposite with 5 wt.% O-M exhibited a smaller amount of stacked plates appeared in the broad- and obscure-shaded region. Similar observations were reported in the literature [19].

Thermal and crystallization behaviors

Table 2 summarized the results from thermal analysis of PBAT and PBAT nanocomposites. The values of crystallinity (X_c) of nanocomposites with organoclay were slightly higher than those of neat PBAT and composites with natural clay, as shown in Table 2. Furthermore, nanocomposites with 1~5% MMT and O-M exhibited higher cooling crystallization temperature (T_{cc}) than neat PBAT. This can be attributed to that the nanofiller can serve as the nucleating agent, making crystallization easier for PBAT, thus increasing T_{cc} as well as X_c [13].

The half crystallization time ($t_{1/2}$) can be calculated as follows [29]:

$$t_{1/2} = (T_{on} - T_{cc})/\chi$$

where T_{on} is the crystallization onset temperature, which is the temperature where the thermograph initially departs from the baseline, T_{cc} is the temperature of the exothermic peak, and χ is the cooling rate (°C/min).

The value of $t_{1/2}$ of neat PBAT was higher than those of nanocomposites. This suggests that the neat PBAT need a longer time to reach the relative crystallinity of 50%. This phenomenon was resulted from the silicate platelets of clay that induced a nucleation and lamellar ordering effect and

Table 2 Results of XRD and thermal analysis for PBAT and PBAT nanocomposites

Composition	2θ (°)	*d* (nm)	T_m (°C)	Xc (%)	T_{cc} (°C)	$t_{1/2}$ (min)	T_d (°C)	UV absorption at 365 nm (%)
MMT	6.77	1.31	–	–	–	–	–	–
O-M	3.19	2.77	–	–	–	–	–	–
PBAT	–	–	133	7.32	92	1.914	354	2.2
PBAT/MMT1	6.42	1.38	133	7.33	106	1.053	357	3.1
PBAT/MMT5	6.40	1.38	135	8.11	99	1.116	377	4.6
PBAT/MMT10	5.58	1.58	132	9.00	96	1.476	372	6.4
PBAT/O-M1	3.08	2.87	131	9.05	105	1.211	388	2.3
PBAT/O-M5	3.08	2.87	132	11.19	104	1.327	387	3.4
PBAT/O-M10	3.06	2.88	132	10.74	97	1.120	374	4.0

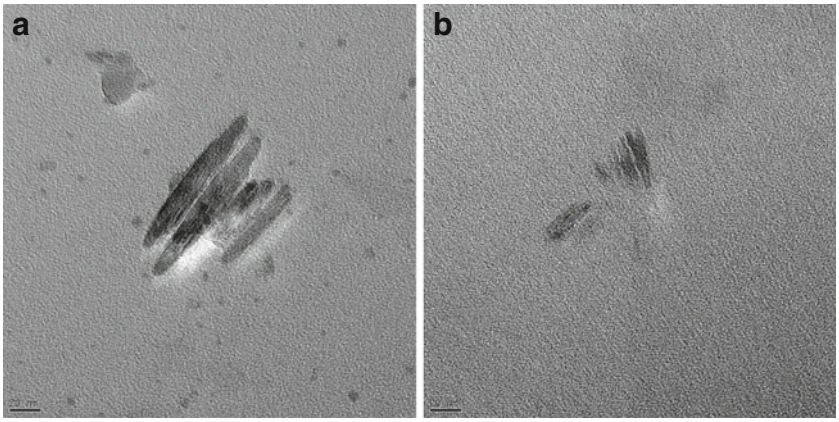

Fig. 3 TEM images of PBAT nanocomposites with inorganic content 5 wt.%: **a** PBAT/MMT, **b** PBAT/O-M

causing the higher crystallization rate of nanocomposites [29]. Furthermore, the crystallinities of O-M series nanocomposites were slightly higher than those of MMT series of nanocomposites, attributing to the finer dispersion of O-M than neat MMT, as shown in Fig. 3.

Thermal stability

Figure 4 shows the TGA curves of PBAT and PBAT nanocomposites with 5 wt.% clay and organoclay contents. The thermal decomposition temperatures (T_d) from the differential thermogravimetry were listed in Table 2. Higher thermal stabilities for nanocomposites with organoclays were observed. The T_d of nanocomposites were 4~34 °C higher than that of neat PBAT (353 °C). The nanocomposite with 1 wt.% O-M exhibited the highest T_d (388 °C). This enhancement in thermal stability was attributed to the barrier effect of the clay layer structure and the strong interaction between the organoclay and PBAT molecules. Furthermore, the clay layer was also supposed to have a shielding effect on the matrix to slow the rate of mass loss of decomposition product [29]. The enhancement in thermal stability is related to the content of organoclay and the dispersion of organoclay in PBAT matrix. When the content of organoclay was at 5 wt.%, agglomeration began to occur, and the barrier effect was decreased. Therefore, the thermal stability of nanocomposites was reduced.

Tensile properties of PBAT composites

Figure 5 shows that the moduli increased with the clay content. This implies that the stiffness of nanocomposite was increased by the addition of clay. The increase can be attributed to the interaction between the nanoparticles and the PBAT matrix. Because of the presence of surfactant, the interaction would be enhanced between O-M particles and PBAT molecules, leading to higher modulus for PBAT/O-

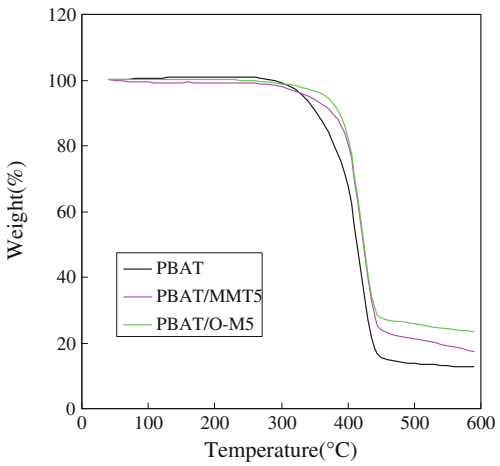

Fig. 4 TGA curves of PBAT and PBAT nanocomposites with inorganic content 5 wt.%

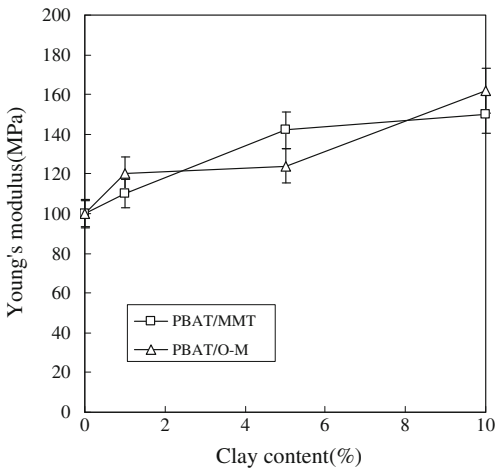

Fig. 5 The tensile properties of PBAT nanocomposites: The dependence of Young's modulus on the clay content

M. However, the modulus of PBAT/O-M5 was lower than that of PBAT/MMT5. This may be attributed to the occurrence of agglomeration in O-M nanoparticles, which may reduce the interfacial area between the polymer matrix and the particles, leading to lower modulus. In the case of PBAT/O-M10, agglomeration may occur for both O-M and MMT, thus the higher modulus may be attributed to the surfactant-enhanced interaction.

Figure 6 shows that the elongation at break decreased with the increase of clay content. This means that the nanocomposite exhibited less ductility than neat PBAT. This can be attributed to the higher crystallinity of the nanocomposites. However, because O-M contained surfactant, lubrication may occur that caused PBAT/O-M exhibiting higher breaking elongation than PBAT/MMT.

Figure 7 shows that the tensile strength of PBAT can be improved slightly by the addition of clay. However, when the clay content was higher than 1 wt.%, the tensile strength began to decrease for PBAT/MMT composites, while the tensile strength of PBAT/O-M remained slightly higher than that of neat PBAT. This agrees with earlier report that the intercalation can reduce the tensile strength [19].

Degradation behavior

Figure 8 shows the values of σ_R of PBAT nanocomposites after UV exposure. Ultraviolet exposure can initiate the reduction of the molecular weight of polymers, thus affecting the biodegradation and biocompatibility of polyesters [30]. In general, the values of σ_R of PBAT/O-M nanocomposites were higher than those of PBAT/MMT nanocomposites at the same clay content, and decreased with the increase of the content of organoclay. This may be due to the smoother surface of PBAT/O-M was able to resist the attack of UV. Furthermore, the absorption of UV light of PBAT/O-M nanocomposites was slightly lower than those of PBAT and PBAT/MMT nanocomposites from Table 2. More absorption of UV light may result in more damage to the PBAT matrix. However, further experiments would be required to clarify the mechanism of degradation under UV light.

Figure 9 shows the rate of hydrolysis for each sample. Basically, the rate of hydrolysis of PBAT was reduced by the addition of clay. This can be attributed to the difference in the crystalline structure of PBAT. The crystallite in neat PBAT was randomly distributed because no nucleating agent was added. Thus the amorphous region was less protected, leading to the highest rate of hydrolysis. Regarding the nanocomposites, the particle size of MMT was larger than that of O-

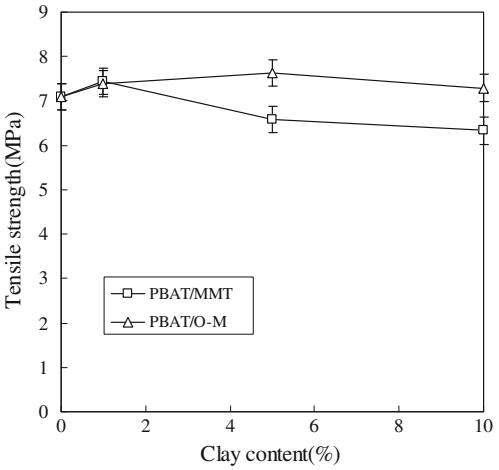

Fig. 7 The tensile properties of PBAT nanocomposites: The dependence of tensile strength on the clay content

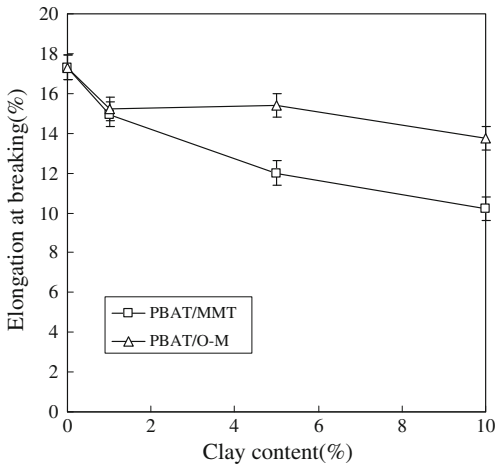

Fig. 6 The tensile properties of PBAT nanocomposites: The dependence of elongation at breaking on the clay content

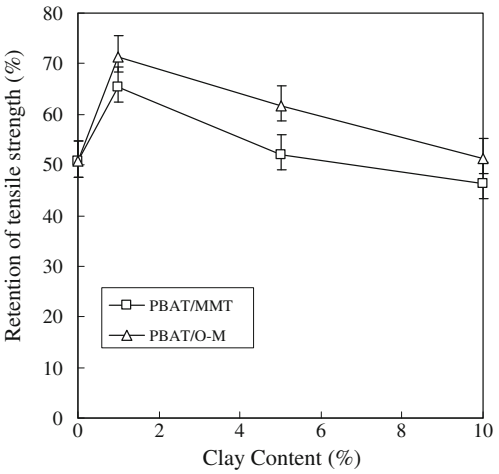

Fig. 8 The retention of tensile strength of PBAT nanocomposites after UV exposure

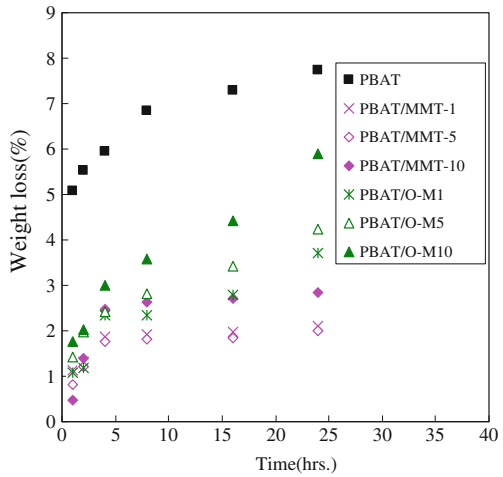

Fig. 9 The hydrolytic degradation of PBAT nanocomposites in 0.1M NaOH

M, as shown in Fig. 3. Since these nanoparticles served as nucleating agent, the crystallite in PBAT/MMT should be larger in size and less in number than that in PBAT/O-M. This made the attack of water more difficult toward PBAT/MMT than toward PBAT/O-M. The other factor affecting the hydrolysis is the hydrophilicity of the sample. Figure 10 shows that the contact angle decreases with the increase of clay content. Thus the rate of hydrolysis increased with the clay content for the nanocomposites of the same series. Furthermore, nanocomposites of PBAT/MMT were more hydrophobic than nanocomposites of PBAT/O-M, probably because of the ODA in O-M. This would hinder the hydrolysis of PBAT/MMT more than PBAT/O-M.

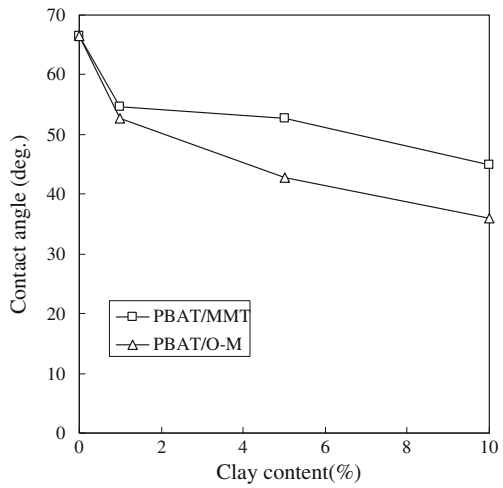

Fig. 10 The water contact angle of PBAT nanocomposites

Water vapor transmission rate

Figure 11 shows the WVTR decreases with the clay content in the nanocompoites. The effect of clays seems to play a barrier role to reduce the transport rate of water vapor. In addition, the values of WVTR of PBAT/O-M were lower than those of PBAT/MMT nanocomposites. This could be attributed to the higher number of crystallites in PBAT/O-M than in PBAT/MMT, resulted in higher tortuosity for water vapor to pass through the film. Because the crystallites in neat PBAT were randomly distributed, the tortuosity should be the least, thus leading to the highest WVTR.

Conclusion

Nanocomposites based on PBAT and montmorillonite nanoparticles were prepared via a solution blending process using chloroform as the solvent. From XRD and TEM observations of PBAT/organoclay nanocomposites, the O-M series exhibited partially intercalated construction. The TGA analysis showed that nanocomposites with nature and modified MMT exhibited higher thermal stabilities than neat PBAT. However, the thermal stability of nanocomposites began to reduce as the content of clay exceeded 5 wt.%. The results of DSC analysis indicated that the organic modified MMT in this study caused a nucleation effect and enhanced the crystallization rate of the PBAT. In addition, the stiffness of nanocomposite was increased by the addition of organoclay and resulted in higher modulus. When exposing to UV irradiation, PBAT/O-M composites exhibited lower degree of degradation than PBAT and PBAT/MMT. By the addition of ODA-modified MMT, the hydrophilicity was increased, while the transmission of water vapor was reduced greatly.

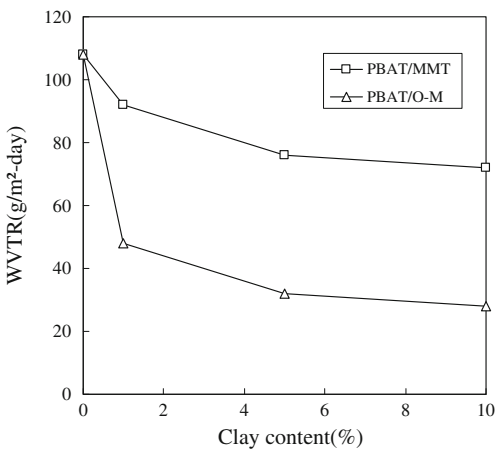

Fig. 11 The water vapor transmission rate of PBAT nanocomposites

References

1. Petrović ZS, Javni I, Waddon A, Bánhegyi G (2007) J Appl Polym Sci 76:133–151
2. Liu X, Wu Q, Berglund LA, Fan J, Qi Z (2001) Polymer 42:8235–8239
3. Rong J, Jing Z, Li H, Sheng M (2001) Macromol Rapid Commun 22:329–334
4. Kim BH, Jung JH, Kim JW, Choi HJ, Joo J (2001) Synth Met 121:1311–1312
5. Vaia RA, Vasudevan S, Krawiec W, Scanlon LG, Giannelis EP (1995) Adv Mater 7:154–156
6. Kim BH, Jung JH, Kim JW, Choi HJ, Joo J (2001) Synth Met 117:115–118
7. Kim BH, Jung JH, Hong SH, Joo J, Epstein AJ, Mizoguchi K, Kim JW, Choi HJ (2002) Macromolecules 35:1419–1423
8. Yeh JM, Liou SJ, Lai CY, Wu PC, Tsai TY (2001) Chem Mater 13:1131–1136
9. Lee D, Lee SH, Char K, Kim J (2000) Macromol Rapid Commun 21:1136–1139
10. Gläsel HJ, Bauer F, Ernst H, Findeisen M, Hartmann E, Langguth H, Mehnert R, Schubert R (2000) Macromol Chem Phys 201:2765–2770
11. Huang JC, Zhu ZK, Yin J, Qian XF, Sun YY (2001) Polymer 42:873–877
12. Strawhecker KE, Manias E (2000) Chem Mater 12:2943–2949
13. Calcagno CIW, Mariani CM, Teixeira SR, Mauler RS (2007) Polymer 48:966–974
14. Chen BQ, Sun K, Ren T (2005) Eur Polym J 41:453–457
15. Matzinos P, Tserki V, Kontoyiannis A, Panayiotou C (2002) Polym Degrad Stab 77:17–24
16. Liu L, Li Y, Liu H, Fang Y (2004) Eur Polym J 40:2739–2744
17. Yang F, Qiu Z (2011) J Appl Polym Sci 119:1426–1434
18. Someya Y, Kondo N, Shibata M (2007) J Appl Polym Sci 106:730–736
19. Someya Y, Sugahara Y, Shibata M (2005) J Appl Polym Sci 95:386–392
20. Witt U, Müller R, Deckwer W (1995) J Environ Polym Degrad 3:215–223
21. Witt U, Müller R, Deckwer W (1997) J Environ Polym Degrad 5:81–89
22. Witt U, Einig T, Yamamoto M, Kleeberg I, Deckwer W, Mülle R (2001) Chemosphere 44:289–299
23. Kijchavengkul T, Auras R, Rubino M, Ngouajio M, Fernandez R (2008) Chemosphere 71:1607–1616
24. Chivrac F, Kadlecova Z, Pollet E, Avérous L (2006) J Polym Environ 14:393–401
25. Diagne M, Guèye M, Vidal L, Tidjani A (2005) Polym Degrad Stab 89:418–426
26. Woo RSC, Chen Y, Zhu H, Li J, Kim JK, Leung CKY (2007) Compos Sci Technol 67:3448–3456
27. Park HM, Lee WK, Park CY, Cho WJ, Ha CS (2003) J Mater Sci 38:909–915
28. Jiang W, Chen SH, Chen Y (2006) J Appl Polym Sci 102:5336–5343
29. Ou CF, Ho MT, Lin JR (2004) J Appl Polym Sci 91:140–145
30. Shangguan YY, Wang YW, Wu Q, Chen GQ (2006) Biomaterials 27:2349–2357